Yanhang Zhang
Department of Aerospace and Mechanical Engineering,
Boston University,
Boston, MA 02215

Martin L. Dunn
Department of Mechanical Engineering,
University of Colorado at Boulder,
Boulder, CO 80309

Kendall S. Hunter

Craig Lanning

D. Dunbar Ivy

Lori Claussen

Division of Cardiology,
The Children's Hospital of Denver,
Denver, CO 80218

S. James Chen
Department of Medicine,
Division of Cardiology,
University of Colorado at Denver and Health Sciences Center,
Denver, CO 80262

Robin Shandas
Department of Mechanical Engineering,
427 UCB,
University of Colorado,
Boulder, CO 80309
and Division of Cardiology,
The Children's Hospital of Denver,
Denver, CO 80218
e-mail: robin.shandas@colorado.edu

Application of A Microstructural Constitutive Model of the Pulmonary Artery to Patient-Specific Studies: Validation and Effect of Orthotropy

We applied a statistical mechanics based microstructural model of pulmonary artery mechanics, developed from our previous studies of rats with pulmonary arterial hypertension (PAH), to patient-specific clinical studies of children with PAH. Our previous animal studies provoked the hypothesis that increased cross-linking density of the molecular chains may be one biological remodeling mechanism by which the PA stiffens in PAH. This study appears to further confirm this hypothesis since varying molecular cross-linking density in the model allows us to simulate the changes in the P-D loops between normotensive and hypertensive conditions reasonably well. The model was combined with patient-specific three-dimensional vascular anatomy to obtain detailed information on the topography of stresses and strains within the proximal branches of the pulmonary vasculature. The effect of orthotropy on stress/strain within the main and branch PAs obtained from a patient was explored. This initial study also puts forward important questions that need to be considered before combining the microstructural model with complex patient-specific vascular geometries. [DOI: 10.1115/1.2485780]

Keywords: pulmonary arterial hypertension, orthotropic hyperelasticity, color M-mode tissue Doppler imaging (CMM-TDI), biplane angiography, 3D pulmonary vasculature

1 Introduction

Pulmonary arterial hypertension (PAH) is an important determinant of morbidity and mortality in children. Secondary PAH results from a known cause whereas primary or idiopathic PAH is a diagnosis of exclusion, indicating absence of known cause. PAH may develop from a multitude of factors including increased pulmonary blood flow as in congenital heart lesions with a left-to-right shunt, left ventricular diastolic dysfunction, or intrinsic vascular changes as in primary PAH. Regardless of etiology, the effect is increased workload on the right ventricle (RV). Children with PAH and/or increased pulmonary blood flow, also develop functional and structural alterations of the pulmonary vasculature [1–4]. Progression of these vascular changes, referred to as pulmonary vascular disease (PVD), largely determines the management and prognosis of these patients and can severely limit surgical repair or long term survival. Pulmonary vascular remodeling, and thus PVD, starts from the onset of abnormal hemodynamics and eventually leads to remodeling of the artery wall. This remodeling process occurs in the upstream arteries as well, leading to arterial wall thickening and extracellular matrix modulation, ultimately resulting in stiffening of the pulmonary arterial walls [5–8].

For both primary and secondary PAH, it is important to accurately diagnose the severity of PAH and consequently the level of afterload imposed on the RV. Hemodynamic measurement of pulmonary vascular resistance (PVR) has been the clinical standard for evaluating pulmonary vascular function and, with the use of novel treatments such as low-dose inhaled nitric oxide and/or prostacyclin agents, evaluating reactivity of the pulmonary vascular bed by measuring changes in PVR upon clinical challenge. Recent studies show that measuring PVR alone may not provide a sufficiently comprehensive metric to evaluate pulmonary vascular reactivity and function; instead, obtaining upstream compliance information either indirectly by measuring the full input impedance of the vascular system, or directly through novel ultrasound tissue Doppler techniques, is needed to more fully quantify RV

Contributed by the Bioengineering Division of ASME for publication in the JOURNAL OF BIOMECHANICAL ENGINEERING. Manuscript received October 7, 2005; final manuscript received August 22, 2006. Review conducted by Yoram Lanir.

afterload [9–12]. In fact, local compliance of the upstream pulmonary arteries (PAs) can significantly modulate pulmonary vascular impedance [10].

Understanding compliance effects is predicated upon elucidating the relationship between structure and mechanical function of the pulmonary arteries. Constitutive models that connect microlevel changes (such as extra cellular matrix remodeling in the arterial wall) and the macrolevel tissue behavior would thus be highly desirable for the diagnosis and treatment of PAH. We have recently developed a statistical mechanics based microstructural finite-element approach to the study of hyperelastic and orthotropic mechanical behavior of upstream PAs [13]. The constitutive model was based on non-Gaussian affine statistical characterization of a network of randomly oriented molecular chains, which mimic structural protein configurations in the extra cellular matrix. The essential idea is that the primary mechanical response of the material is due to an underlying molecular network structure, which relates applied deformation to linking and geometric structure of individual molecular chains. The network is composed of eight-chain unit elements [14,15], with the deformation of each molecular chain governed by an entropy-based constitutive law. The model provides an analogy between the entangled long molecular chains and the structural protein framework seen in the medial layer.

We have shown that this model is capable of resolving the experimentally measured pressure-stretch data from normotensive and hypertensive rat main pulmonary artery (MPA), proximal left pulmonary artery (LPA), and right pulmonary artery (RPA), and is useful for investigating deformation, stress resultants, and nonlinear material properties. More importantly, the application of such a microstructural model to the study of PA mechanics allows links to be studied between the macrolevel mechanical response to the deformation (entropy change) of individual molecular chains at the microlevel. For example, our animal study provoked the hypothesis that increased cross-linking density of the molecular chains may be one biological remodeling mechanism by which the PA stiffens in PAH [13].

One of our next goals is to apply this model to patient-specific clinical studies using a combination of the existing microstructurally based finite element model and established clinical research capabilities to understand the relationship between fundamental arterial biomechanical changes and the development of PAH. Since to the best of our knowledge such implementation has not been performed before, several questions regarding application of the material parameters derived from prior animal studies to the clinical simulations, the most appropriate choice of simulation parameters, such as boundary and initial conditions, material assumptions, such as isotropy and anisotropy, and validation using clinical data, remain to be addressed before the model can be used for clinical predictions. In this paper we perform validations using clinically measured pressure–diameter responses at the RPA, and explore the effect of orthotropy on stress/strain within the main and branch PAs obtained from a patient. We begin by describing briefly the constitutive model, followed by implementation of the model to clinical data with validation, and finally application of the model to patient-specific three-dimensional images.

2 Methods

2.1 Constitutive Modeling and Finite-Element Implementation. The statistical mechanics based microstructural model was originally developed by Arruda and Boyce [14] for isotropic hyperelasticity and modified by Bischoff et al. [15] to incorporate orthotropy. The eight-chain element was selected as the basic unit; these can have different dimensions in the three orthogonal material directions and in this manner, the response of the unit element is made orthotropic. Figure 1 shows the schematic of the artery wall and the eight-chain orthotropic unit element to model the orthotropic behavior of the synthetic network structure in the medial layer. The fundamental component of the network structure of the artery wall in the model is a unit element, which is characterized by three orthogonal unit vectors, **a**, **b**, and **c**, representing principal material directions. In each unit element, eight molecular chains are situated along the diagonals of the unit element and linked together at the center of the element. The chains deform with element deformation. As the material deforms, each unit element, and thus the eight constituent molecular chains, will be deformed. Each chain is treated as a macromolecule, which is modeled as a freely joined chain. The strain energy of each unit element is associated with the entropy change of the chains. The unit element can then be homogenized to form the strain energy function of the material. Interested readers are referred to Bischoff et al. [15] for details regarding the development of the model. The final form of the strain energy function is [15]

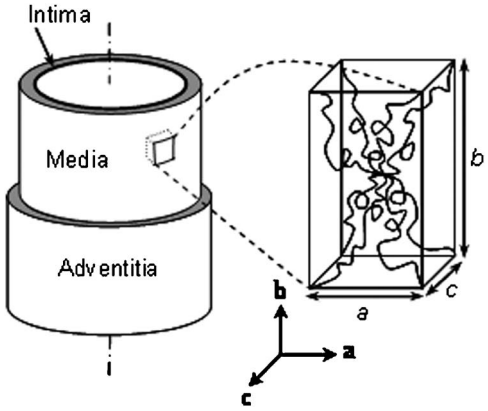

Fig. 1 Schematic of the artery wall and the eight-chain orthotropic unit element to model the orthotropic behavior of synthetic network structure in the intimal-medial layer

$$w = w_0 + \frac{nk\Theta}{4}\left[N\sum_{i=1}^{4}\left(\frac{\rho^{(i)}}{N}\beta_\rho^{(i)} + \ln\frac{\beta_\rho^{(i)}}{\sinh\beta_\rho^{(i)}}\right) - \frac{\beta_p}{\sqrt{N}}\ln(\lambda_{\mathbf{a}}^{a^2}\lambda_{\mathbf{b}}^{b^2}\lambda_{\mathbf{c}}^{c^2})\right] + B[\cosh(J-1)-1] \quad (1)$$

where w is the overall energy; w_0 is a constant; B is a parameter that controls the bulk compressibility; and J is the volume ratio. Parameters a, b, and c are normalized dimensions along the principal material directions, and $\lambda_{\mathbf{a}}$, $\lambda_{\mathbf{b}}$, and $\lambda_{\mathbf{c}}$ are stretches along these directions. $N=a^2+b^2+c^2/4$ is the number of rigid links within each individual chain. $\sqrt{N}$ defines the extensibility of the chain, i.e., as the chain stretch approaches $\sqrt{N}$, the stiffness increases dramatically, thereby resulting in the strain-stiffening response of the macromolecule; $\rho^{(i)}$ are the normalized deformed lengths of the constituent chains in the unit element; $\beta_\rho^{(i)} = \ell^{-1}(\rho^{(i)}/N)$, and $\ell(x)=\coth x - 1/x$ is the Langevin function; and $\beta_p=\ell^{-1}(p/N)$, where $p=1/2\sqrt{a^2+b^2+c^2}$ is the initial normalized length of each chain. Parameter n is the chain density per unit volume; k ($=1.38\times10^{-23}$ J/K) is Boltzmann's constant; and Θ ($=298$ K) is absolute temperature. Note that $nk\Theta$ defines the initial stiffness, and B is significantly greater than $nk\Theta$ to model the nearly incompressible material behavior.

Details of the finite element implementation of the constitutive model and its experimental application are presented elsewhere [13]; only basic aspects are shown here. A customized user material subroutine was created to prepare the problem for finite-element solution, which involves determination of the Cauchy stress and elasticity tensor in the deformed configuration [16]. Shell elements (general purpose with reduced integration (SR4)) were used for modeling since such elements resemble the geometric characteristics of the artery wall where the dimension in the thickness direction is much smaller than that along the other two directions. Furthermore, the inherent plane stress assumption for

shell elements greatly simplifies the equations and facilitates solution convergence for this nonlinear problem, especially when combining the complex material model with patient specific three-dimensional (3D) anatomy. However the use of shell elements should be with caution in the case of a thicker vessel wall, for which the shell simplification may not be valid.

2.2 Clinical Studies

2.2.1 In Vivo Measurement of Instantaneous PA Pressure-Diameter (P-D) Response. All institutional policies (HIPPA/COMIRB) were followed during data collection and analysis, and the institutional board approved all studies. Developing patient-specific simulations with our recently developed microstructural model requires validation to ensure the model reproduces physiological conditions. Determining which particular clinical measurements to use for validation is nontrivial since such measurements will need to be easily obtained yet still represent an accurate metric for evaluating mechanical response. All patients with PAH at the Denver Children's Hospital are routinely evaluated in the cardiac catheterization laboratory where invasive measurements of PA pressures are obtained. We have recently developed a simple method to combine such pressure (P) measurements with ultrasound measurements of PA diameter (D) and quickly obtain P-D curves for each patient [12]. Obtaining P-D data for each patient allows the finite element model to be validated at one location, which should provide confidence regarding the accuracy of the computed deformations over the rest of the pulmonary vasculature.

Instantaneous pressure in the RPA was measured using a fluid-filled catheter and the instantaneous diameter of the same artery was obtained using the ultrasound color M-mode tissue Doppler imaging (CMM-TDI) technique [12]. Custom software was used to extract the instantaneous diameter of the RPA from the CMM-TDI images. Since the focus of this paper is on the development of the methodology to combine the statistical mechanics based constitutive model and clinical studies, only illustrative clinical data are included.

2.2.2 3D Reconstruction of Pulmonary Vascular Anatomy Using Biplane Angiographic Images. We have adapted a method originally developed by Chen and Carroll [17] to reconstruct 3D adult coronary vascular anatomy from biplane angiographic images for the pediatric pulmonary vasculature. The method utilizes custom software to determine the centerline and local diameter of the branched pulmonary vasculature from the biplane images to create the initial skeleton of the vascular tree. This skeleton is then converted into a 3D solid model of the arterial lumen. Since the method does not provide information on arterial wall dimensions, wall thickness is added as 10% of local diameter [18]. See Sec. 2.3 for details on determination of the wall thickness on a node by node basis. The MPA, LPA, and RPA were included in these models. The method allows images to be collected at any point during the cardiac cycle; in these studies images were taken at middiastole, since this represented the baseline condition for the modeling studies.

2.3 Finite-Element Modeling

2.3.1 P-D Response. To validate the finite-element model with clinical data, the in vivo P-D response of the RPA was modeled via inflation of a tube under uniform pressure. The use of shell elements induces the assumption that the RPA is a thin-walled cylindrical tube. The radial stress is assumed to be zero, and only average and uniform hoop stress and axial stress is calculated. To study the effect of axial stretch, the tube is first stretched in the longitudinal direction ($\lambda_z = 1 - 1.5$) and then inflated [19,20]. During inflation, both ends are fixed in their planes but are free to move in the radial direction. The initial thickness of the tube is assumed to be 10% of the center diameter of the artery [18], and the length of the tube is assumed to be ten times the wall thickness, although the length of the cylinder is inconsequential when a uniform axial stretch is imposed [20].

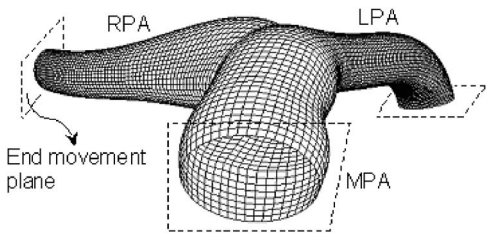

Fig. 2 Finite element mesh of a 3D patient-specific proximal pulmonary vascular structure reconstructed from biplane angiography images. Three end movement planes are applied to constrain the movement of the 3D anatomy. The nodes at the ends of the MPA, LPA, and RPA are allowed to move only in the end movement plane.

2.3.2 3D Pulmonary Vasculature. Subsequent to validation, finite-element simulations were run on a patient-specific 3D model of the pulmonary vasculature. Three-dimensional geometric reconstructions obtained from clinical images were meshed at the artery midplane and transferred into ABAQUS, where we have implemented the orthotropic hyperelastic constitutive model of the pulmonary arterial wall. To prepare the finite element model of patient-specific 3D anatomy, appropriate boundary conditions are important especially for stress/strain analysis. Figure 2 shows the boundary conditions in the finite-element model and the mesh of the 3D anatomy. Three end movement planes, defined by three nodes on the end, are applied at the end of the PAs to remove the rigid body motion and constrain the movement of the ends. At each end, the nodes are allowed to move only in the respective end movement plane. Although the boundary conditions applied this way may be different from the realistic situation, we believe this provides a reasonable balance between using fully fixed ends, which induce highly artificial end effects, and allowing accurate physiological motion for these upstream arteries. The wall thickness in the finite-element model of 3D anatomy using shell elements was set on a node-by-node basis. A customized program was used to identify the diameter and assign thickness at each node. The process proceeds by first computing the minimum distance from a particular node to each branch skeleton centerline to determine the node's proximity to each branch. With these distances the node is then associated with one or both branches; an association exists if the node-to-centerline distance is less than 125% of the centerline radius at the corresponding location. For a single association, the wall thickness at the node was taken to be 10% of the corresponding centerline diameter [18]. Near the junction, the nodes associate with both branches, and the thickness is assumed to be 10% of the average of the two centerline diameters. Figure 3 shows the contour of arterial wall thickness of a 3D pulmonary vascular anatomy. A uniform and average static pressure was applied inside the arterial wall to simulate the pressure loading over the cardiac cycle. Local coordinate systems are defined in the MPA, LPA, and RPA to align the local material directions with the circumferential, longitudinal, and transmural directions of the arterial wall, especially for orthotropic material. To define the local coordinate systems, the 3D pulmonary vasculature is divided into sections to approximate the smooth curve of the centerline with line segments. Local coordinate systems are then defined within each section of the 3D pulmonary vasculature.

2.4 Input Material Parameters. Input material parameters in the finite element models are based on our previous studies comparing experimentally measured pressure-stretch data against model predictions for a rat model of PAH [13]. Averaged material parameters (chain density=n and number of rigid links within

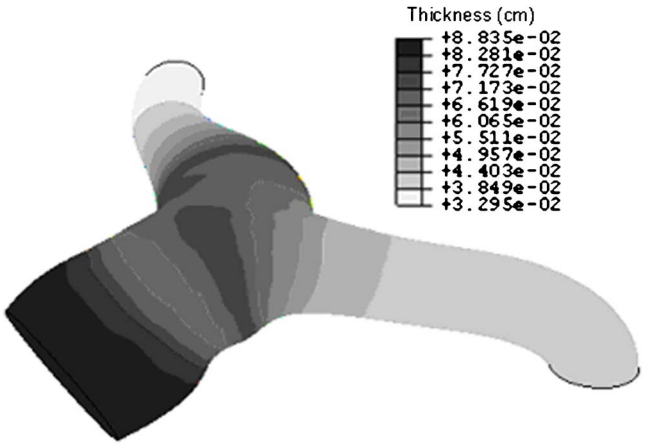

Fig. 3 Input wall thickness of the finite-element model of the 3D patient-specific pulmonary vascular structure

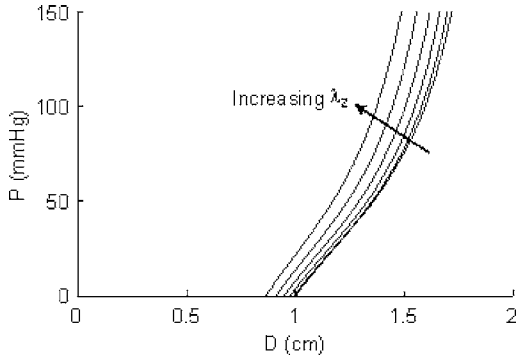

Fig. 4 Predicted *P-D* responses using a simple tube inflation model. The artery wall is assumed to be isotropic with material parameters HI from Table 1. Curves from right to left correspond to axial stretch λ_z from 1.0 to 1.5 in increments of 0.1.

each chain=N) under normotensive and hypertensive conditions are used in the current studies. Normalized eight chain unit element dimensions a, b, and c are related to N by $N=a^2+b^2+c^2/4$, and are aligned with the circumferential, longitudinal, and transmural directions of the PAs, respectively. For the studies of the 3D pulmonary vasculature, we assume that the material properties of MPA, LPA, and RPA are the same. Both isotropic and orthotropic material properties are considered in the finite element modeling. See Table 1 for a summary of material parameters used in this study.

In this study, only material properties of the intimal-medial layer are considered in the finite-element model for several reasons. First, both our previous experimental and modeling studies on rat PAs were performed with the adventitial layer removed, thus only material parameters of the intimal-medial layer are available; second, we did not wish to complicate this initial study by incorporating the adventitial layer; and third, several prior experimental studies [21–23] indicate that the medial layer is stiffer than the adventitial layer. In particular, von Maltzahn [21] measured mechanical properties of the bovine carotid arteries before and after the outer layers were peeled away. They found that the media is stiffer, more nonlinear, and subjected to higher stresses than commonly assumed; and both the medial and adventitial layers are anisotropic and stiffer in the axial direction than in the circumferential direction. Yu et al. [22] performed bending experiments on pig thoracic aortas to investigate the mechanical properties of different layers of blood vessels without physically separating the layers. They found that the Young's modulus of the medial layer is about an order of magnitude higher than that of the adventitial layer. These studies suggest that the intimal-medial layer, consisting of endothelial and smooth muscle cells and elastic lamina within the extra cellular matrix, may be the dominant regulator of mechanical response in the artery.

Table 1 Material parameters used in the finite element simulations. Four groups of material parameters are listed in the table.

		Material parameters			
Groups	n ($1/mm^3$)	a	b	C	N
NI[a]	7.99×10^{15}	1.77	1.77	1.77	2.35
HI[b]	6.57×10^{15}	1.49	1.49	1.49	1.67
HOL[c]	6.57×10^{15}	1.2	2.1	0.9	1.67
HOC[d]	6.57×10^{15}	2.1	1.2	0.9	1.67

[a]NI=normotensive isotropic.
[b]HI=hypertensive isotropic.
[c]HOL=hypertensive orthotropic, stiffer in longitudinal direction.
[d]HOC=hypertensive orthotropic, stiffer in circumferential direction.

3 Results

3.1 Validation of the Model Using *P-D* Data. We first studied the *P-D* responses and stresses at different axial stretches using a simple cylindrical tube model. The tube is first subjected to an axial stretch $\lambda_z(1-1.5)$ and then inflated under uniform pressure up to 150 mm Hg. Figure 4 shows the predicted *P-D* data in which the tube is assumed to have an initial diameter $D=1$ cm. Averaged input material parameters of rats with PAH are used in this model, and the artery wall is assumed to be isotropic. Orthotropy and its effect on the structural responses and detailed strain patterns will be included and discussed in the fully 3D pulmonary vasculature studies. Figures 5(a) and 5(b) show corresponding circumferential and longitudinal stresses versus diameter for the *P-D* responses in Fig. 4.

We then built a "validation map" to provide a rough validation for applying material parameters from our previous animal studies to the PAs of children with PAH. Figure 6 shows this "validation map" and clinical *P-D* measurements at the RPA of children. In the finite element simulations, we use average material parameters of both normotensive and hypertensive rats from Table 1. The arterial wall is again assumed to be isotropic. Tubes with diameter $D=0.75$ cm, 1 cm, and 1.25 cm are modeled to approximate the arterial diameters of patients of different ages. The axial stretch λ_z is fixed at 1. At each diameter, simulations are done with two sets of averaged material parameters of normotensive (dashed lines) and hypertensive (solid lines) rats. Figure 6 also displays *P-D* loops of a normotensive subject and a patient with PAH. The *P-D* loop of the patient with PAH has a steeper slope that follows the orientation of the solid lines, while the *P-D* loop of the normotensive subject has a smaller slope that follows the orientation of the dotted lines.

3.2 3D Pulmonary Vasculature. Figures 7–9 show contours of stress/strain distribution in the MPA, LPA, and RPA when subjected to uniform pressures. All of the contours are evaluated at the midplane of the arterial wall and diplayed in local coordintate systems defined by the MPA, LPA, and RPA. Cauchy stress and logarithmic strain is used to generated the contours. Figure 7 shows contours of longitudinal strain. The arterial wall of the pulmonary vasculature is assumed to be isotropic (HI in Fig. 7(a)), orthotropic and stiffer in the longitudinal direction (HOL in Fig. 7(b)), and orthotropic and stiffer in the circumferential direction (HOC in Fig. 7(c)). In Fig. 7(a), when the arterial wall is assumed to be isotropic, the resulted longitudinal strain is mainly positive except for a few locations as indicated by the dark areas.

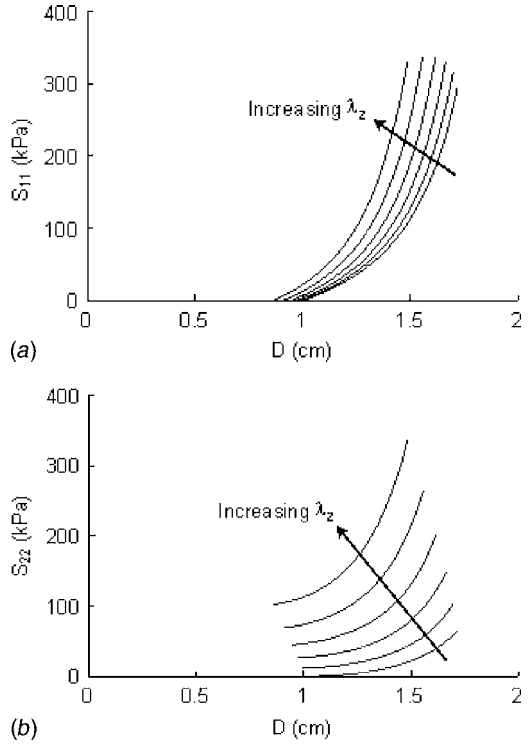

Fig. 5 Predicted (*a*) circumferential and (*b*) longitudinal stresses versus diameter for the *P-D* responses in Fig. 4. Axial stretch λ_z is increased from 1.0 to 1.5 in increments of 0.1.

Highest longitudinal strain occurs at both superior and inferior junctions of the three PAs. In Fig. 7(*b*), when the arterial wall is assumed to be orthotropic and stiffer in the longitudinal direction, large areas of negative logitudinal strain manifests. This negative strain appears at very low pressure and increases in magnitude with pressure. Highest longitudinal strain again happens at both the superior and inferior junctions of the three PAs. In Fig. 7(*c*),

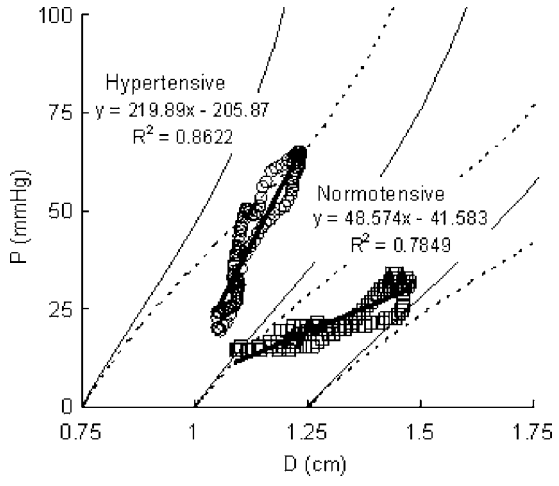

Fig. 6 *P-D* loops of a normotensive subject (squares) and a hypertensive patient (circles). Linear regression lines of pressure versus diameter for each loop are also shown. Simulations were based on a tube inflation model. Solid lines correspond to simulations using material parameters HI and dashed lines correspond to simulations using material parameters NI from Table 1. Initial diameters of the tube vary from 0.75 cm to 1.25 cm to account for the different sizes of the arteries due to the different ages of the patients.

when the arterial wall is assumed to be orthotropic and stiffer in the circumferential direction, the longitudinal strain is all positive. Highest longitudinal strain occurs at the inferior junction of three PAs and the junction between MPA and LPA, and between MPA and RPA. Figure 8 shows corresponding contours of circumferential strains, which are all positive; higher strains still occur at the junction of PAs. Contours of stress components are shown in Fig. 9 for isotropic arterial wall assumptions. The arterial wall is under a biaxial stress state, therefore the overall contour pattern for each stress component is determined by both the corresponding strain component and the Poisson's effect.

Figure 10 shows predicted *P-D* response at the midpoint of the RPA of the 3D pulmonary vasculature simulations in Figs. 7–9 for the conditions of isotropy and orthotropy discussed above. Effect of wall thickness on the predicted *P-D* responses is also shown for the condition of isotropy.

4 Discussion

This work represents the first application of a microstructural orthotropic hyperelastic model to the clinical study of PA mechanics in children with PAH. A finite-element approach was adopted to implement the model. Material parameters determined from our previous studies via comparing model output to measured pressure-stretch results from normotensive and hypertensive MPA, LPA, and RPA obtained from a rat model of PAH [13] were used in the study of PA mechanics in children. The long-term goal of this study is to understand the relationship between fundamental arterial microstructural changes and development of PAH and to use this information to develop clinically meaningful yet fundamentally based diagnostics for evaluating pulmonary vascular function noninvasively. This should be useful in following disease progression, especially regarding the initiation and effects of arterial remodeling in PAH, and in more accurately estimating pulmonary vascular reactivity in patients undergoing pulmonary vasodilator challenge as is routinely done at our institution [10].

In our previous study, the material parameters in the microstructural model were determined based on biomechanical test on the medial layer of the PAs of rats with and without PAH [13]. For the medial layer consisting of elastin-based laminae surrounded by extra-cellular matrix and smooth muscle cells, the microstructure can be represented as a tangled molecular network with individual molecular fibers connected to each other via cross-linking and entanglement. Although the eight-chain network model does not represent the actual organization/alignment of the protein fibers in the arterial wall, the molecular chains in the model represent the functional equivalent in a mechanical sense of the fiber network found in the medial layer. We have shown that the mechanical response of the medial layer is captured well by the entropic elasticity of a network of molecular chains. More importantly, because the material parameters in the microstructural model possess physical meanings, our previous study provoked the hypotheses that increase of cross-linking density might be a key mechanism by which pulmonary artery stiffens in PAH. Interested readers are referred to Zhang et al. [13] for detailed discussions. Briefly, our previous results suggest that compared to normotensive conditions, hypertensive PAs showed no significant change in the chain density per unit volume (material parameter *n* in Table 1); however, chain extensibility decreased significantly (material parameter *N* in Table 1). The decrease in chain extensibility indicates that the mean spacing between molecular links has decreased in the hypertensive case, and implies greater degree of molecular cross-linking within, for example, elastin fibers to both other elastin fibers and/or to other structural protein fibers or smooth muscle cells found in the medial extra-cellular matrix. Although our efforts have focused initially on the medial layer of the arterial wall, it is important to recognize that the arterial wall is a complex multilayered structure and other components will contribute to its mechanical behavior as well. Subsequent models

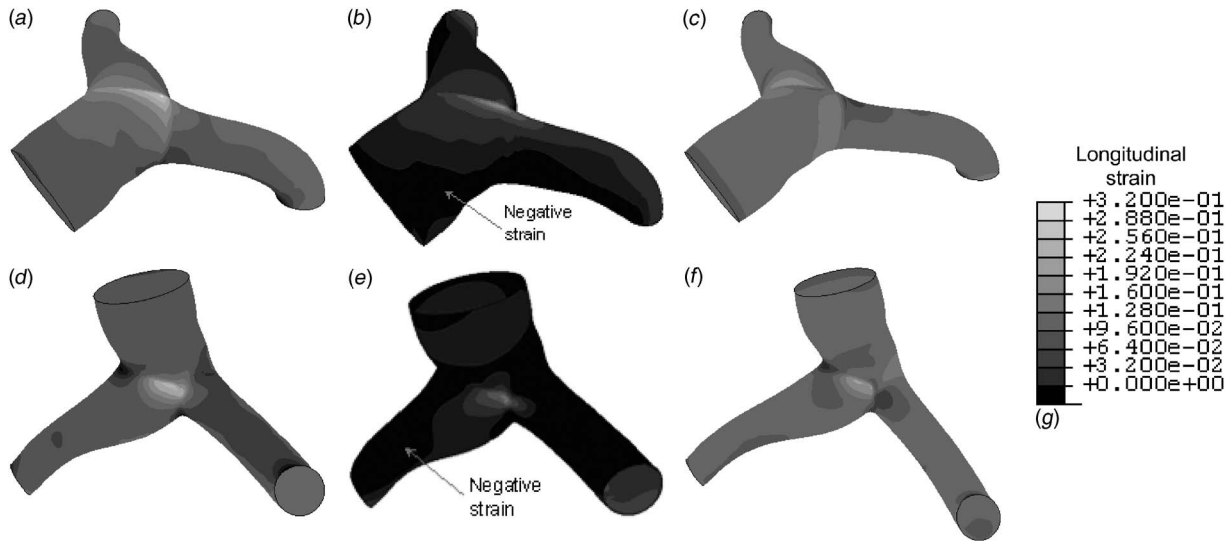

Fig. 7 Contours of longitudinal strain (*a*) at pressure of 40.5 mm Hg when the artery wall is assumed to be isotropic with material parameters HI from Table 1; (*b*) at pressure of 40.5 mm Hg when the artery wall is assumed to be orthotropic and stiffer in the longitudinal direction with material parameters HOL from Table 1; and (*c*) at pressure of 39.6 mm Hg when the artery wall is assumed to be orthotropic and stiffer in the circumferential direction with material parameters HOC from Table 1

are being developed to allow inclusion of collagen fibers and smooth muscle cells and thereby expand the mechanical description of the artery wall.

4.1 Validation of the Model. Currently, the ability to obtain detailed spatially and temporally resolved clinical data are limited. Several diagnostics are performed on these patients; we routinely measure mean hemodynamics (PVR, cardiac output, mean pressures), vascular input impedance and pressure–diameter curves in the pulmonary vasculature for all patient studies in the catheterization laboratory [10,12]. The *P-D* response of the RPA is an easily implemented method of evaluating structural response of the upstream arteries under vasodilator challenge. The *P-D* response was thus used in this work to validate the finite element modeling (Fig. 6). We use a simple tube model for the validation, since our primary interest here is on the pressure–diameter response rather than detailed stress/strain distribution. In addition, the use of clinical *P-D* data, albeit only for the RPA, provides an initial approach to the issue of validation for complex vascular structures under in vivo conditions. The orientations of the clinical *P-D* loops of normotensive and hypertensive arteries agree reasonably with the *P-D* responses using material parameters based on animal studies [13]. The hypertensive *P-D* loop has higher mean PA pressure and steeper loop orientation, and the hypertensive *P-D* loop shifts to the left of the normotensive loop. This indicates that passive changes, i.e., movement of the *P-D* loop along the nonlinear stress–strain curve as pressure varies [24–26]

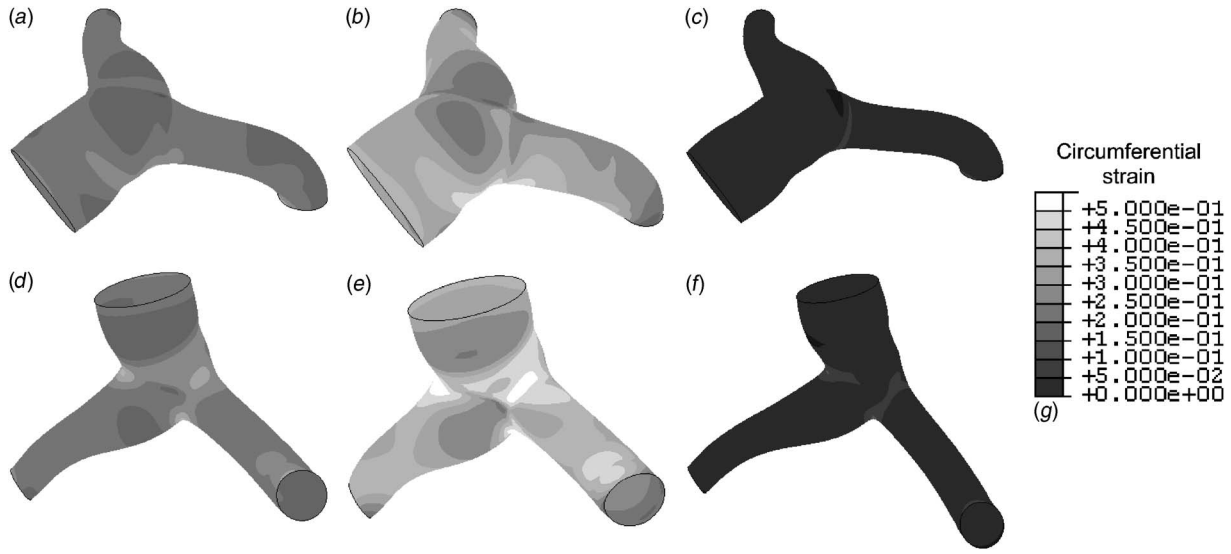

Fig. 8 Contours of circumferential strain (*a*) at pressure of 40.5 mm Hg when the artery wall is assumed to be isotropic with material parameters HI from Table 1; (*b*) at pressure of 40.5 mm Hg when the artery wall is assumed to be orthotropic and stiffer in the longitudinal direction with material parameters HOL from Table 1; (*c*) at pressure of 39.6 mm Hg when the artery wall is assumed to be orthotropic and stiffer in the circumferential direction with material parameters HOC from Table 1

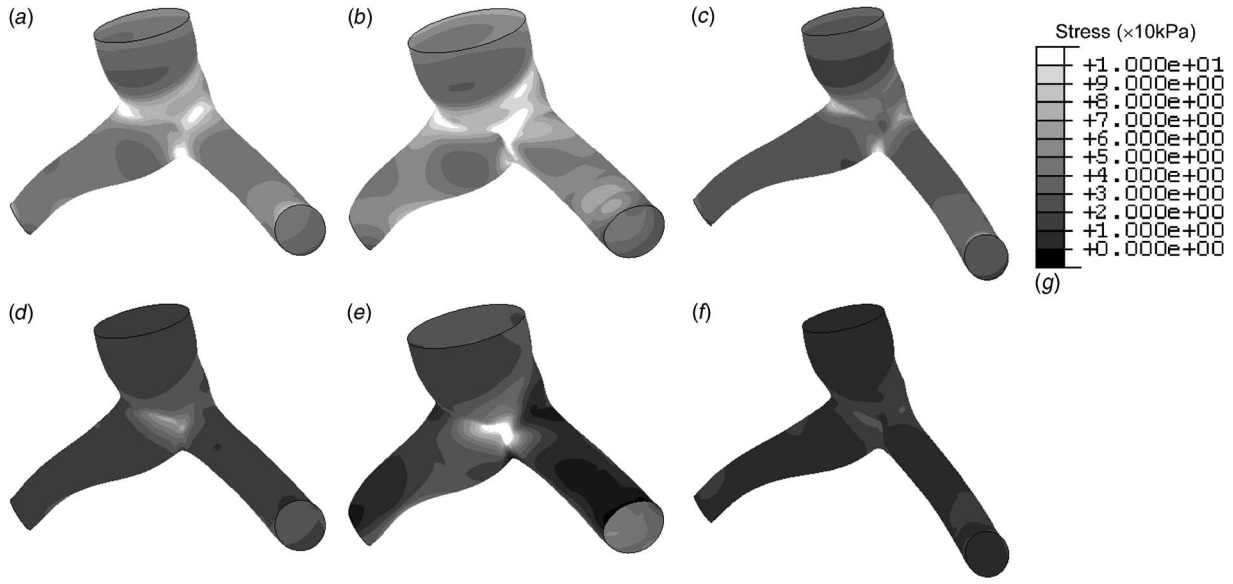

Fig. 9 Contours of stresses in the circumferential (left) and longitudinal (right) directions: (*a*) at pressure of 40.5 mm Hg when the artery wall is assumed to be isotropic with material parameters HI from Table 1; (*b*) at pressure of 40.5 mm Hg when the artery wall is assumed to be orthotropic and stiffer in the longitudinal direction with material parameters HOL from Table 1; (*b*) at pressure of 39.6 mm Hg when the artery wall is assumed to be orthotropic and stiffer in the circumferential direction with material parameters HOC from Table 1

is not the only mechanism involved in clinical manifestation of stiffened pulmonary arteries. Other mechanisms such as structural remodeling and active myogenic effects (increase in smooth muscle tone) may also play important roles. Our previous work provoked the hypothesis that cross-link density is one mechanism by which structural remodeling may take place in the hypertensive pulmonary artery [13]. Results presented here appear to further confirm this hypothesis since varying molecular cross-linking density in the model allows us to simulate the changes in the *P-D* loops between normotensive and hypertensive conditions reasonably well, as shown in Fig. 6. However, active mechanisms such as smooth muscle relaxation and/or constriction can also change the intrinsic elastic properties of the PAs, and thereby produce a shift of the *P-D* loop [26]. It is likely a combination of such effects that dictate the ultimate structural characteristics of these arteries. Combining clinical data extraction of the *P-D* loop under baseline and challenge conditions with finite-element modeling studies should thus provide heretofore unavailable clues regarding structural remodeling changes of the pulmonary artery in the clinical manifestation of pulmonary hypertension.

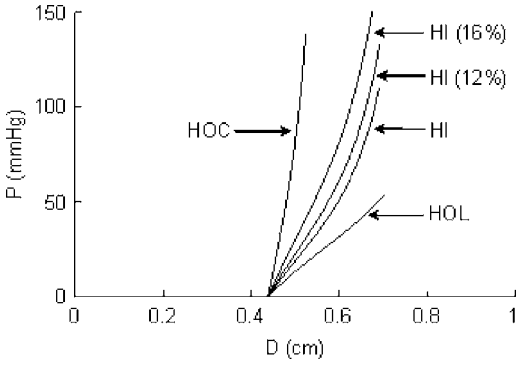

Fig. 10 Predicted *P-D* responses at the midpoint of RPA when the artery wall is assumed to be isotropic with material parameters HI, orthotropic and stiffer in the longitudinal direction with material parameters HOL, and orthotropic and stiffer in the circumferential direction with material parameters HOC from Table 1. Sensitivity study on the thickness of the arterial wall was performed by increasing the nodal thickness from 10% (HI) to 12% and 16% of the local diameter.

4.2 Effect of Initial Conditions: Axial Stretch. The axial stretch affects the *P-D* response of the artery, as well as the stresses in the arterial wall (Figs. 4 and 5). Basically, as the axial stretch increases, the artery becomes stiffer in the circumferential direction, which is manifested by the *P-D* curves. Stresses increase in both the circumferential and longitudinal directions. Movement of the heart may possibly cause stretch/twist of the pulmonary vasculature before or during inflation; this effect is not included in this study but is a topic of future research.

4.3 Effect of Initial Conditions: Material Orthotropy. Although in the validation of the model we used averaged material parameters, (n,N), and assumed the arterial wall to be isotropic (Fig. 6), we did observe obvious anisotropic response in the longitudinal and circumferential directions of many proximal PAs in our previous animal study [13]. Orthotropy of the artery has also been demonstrated and studied both experimentally and theoretically on animals by other research groups [21,27,28]. Study of bovine carotid arteries by von Maltzahn [21] suggests that both the medial and adventitial layers are stiffer in the axial direction than in the tangential direction. Zhou and Fung's study [27] on thoracic aortas of dogs indicates that the longitudinal stress–strain curve turns nonlinear at a smaller strain and has as a steeper nonlinear region than the circumferential stress–strain curve does. Studies of pulmonary arteries of rats with PAH by Drexler et al. [28] show that most of the MPAs are stiffer in the circumferential direction and almost all of the LPAs and RPAs are stiffer in the longitudinal direction. In this study, we assume that the PAs have the same material properties in a 3D vascular system. However it is possible in one patient that the PAs may have a different orthotropy trend. Our validation based on *P-D* responses at the RPA cannot resolve this complex issue. Further work using more advanced imaging techniques such as magnetic resonance tissue tagging to examine arterial strain patterns should shed further light on this topic.

To study the effect of orthotropy on 3D pulmonary vascular mechanics, the chain density (n) and chain length (N, number of

rigid links within each chain) is kept the same, and the normalized unit element dimensions (a, b, and c) are varied, which at the microlevel results in changing the spatial orientation of the macromolecular chains in the arterial wall, and at the macrolevel results in changing the material property, i.e., cylindrical orthotropy. Since a and b are aligned with the circumferential and longitudinal direction of the arterial wall, the angle ArcTan$[b/a]$ reflects the projection of the macromolecular chains onto the arterial wall. This perspective is similar to Holzapfel's constitutive model [29], in which each layer is considered as a composite reinforced by two families of fibers that are arranged in symmetrical spirals. In their model, fiber angle is defined as the angle between the fibers and the circumferential direction of the artery. The fiber angles in Figs. 7–9 correspond to 45 deg, 60.3 deg, and 29.7 deg. In Holzapfel's multilayer consitutive model of the arterial wall, this angle was assumed to be 29 deg in the media and 62 deg in the adventitia, based on the work from Xie et al. [23].

Considering the artery wall as a cylindrically orthotropic material results in different stress/strain patterns within the 3D vasculature, as shown in Figs. 7–9. Different *P-D* responses can result purely due to the orthotropy in the arterial wall, as shown in Fig. 10. Many three-dimensional finite-element simulations of arteries [19,20] have focused more on residual stresses and assumed the artery to be isotropic. Whether anisotropy should be included in such models is an important question, especially given the increased complexity this adds to the model, Our studies show marked differences in stresses and strains within the branched vasculature between isotropic and orthotropic conditions, which might be important, since physiologically fibroblasts, smooth muscle cells and a variety of precursor cells may alter function based on local material stresses and strains [1]. Thus, further studies on linking the change in artery mechanics to remodeling, and obtaining further clinical data to more completely investigate this issue are necessary.

Note that the boundary conditions of applying movement planes at the ends allow the deformed shape of the 3D vasculature to differ for different anisotropy assumptions. For example in Fig 7, more longitudinal elongation is presented in Fig. 7(c) than in Fig. 7(a), and longitudinal shortening is seen in Fig. 7(b). When the material is assumed to be orthotropic and stiffer in the longitudinal direction (HOL), it is difficult for the vasculature to be stretched in the longitudinal direction. Therefore when the vasculature is inflated, the diameter of the artery increases and the ends expands in the circumferential direction. The combination of the constriction of the end movement plane and expansion of the PA produces negative longitudinal strain as shown in Fig. 7(b).

It is also useful to address the assumption of local wall thickness being 10% of local diameter. Our biplane angiography method does not provide information on wall thickness. We are examining other methods such as 3D MRI, which can provide such information; however this work is still in its early stages. At the pressure of 26 mm Hg, increasing the wall thickness by 60% results in a change of about 6% in the wall diameter (by comparing HI and HI (16%) in Fig. 10), which is comparable to the total deformation, about 20% of the initial diameter. It is interesting to note that changing material properties from isotropic to orthotropic produces more variation in the results than changing wall thickness.

4.4 Limitations in Our Study. It is important to recognize the limitations in our study. Prediction of patient-specific pulmonary artery mechanics is based on a microstructural constitutive model developed from testing of rat pulmonary arteries. Only material properties of the intimal-medial layer are considered in the finite element model, which may underestimate the stiffness of the PA. Modeling of the 3D pulmonary vasculature involves many complicated issues such as artery geometry, appropriate boundary and loading conditions, residual stresses, and unknown material properties. Given the absence of detailed information on patient-specific arterial wall material properties, cross-sectional geometry of the patient's vascular system, etc., available using current clinical diagnostics, we assume the initial cross section of the artery to be circular, and the wall thickness to be 10% of the local diameter. Our current efforts using magnetic resonance imaging (MRI) to resolve the details of arterial wall geometry in patients should provide a means to verify and/or refine these assumptions.

Uniform pressure was used and pressure drop in the vascular tree is not considered. Movement of the heart, which may produce deformation, such as stretching and twisting, of the PAs is currently under study and not included in this work. For the orthotropic assumption, the alignment of the local material directions in the artery wall, especially at the junctions of branches, is unknown and its effect on the local stress/strain field needs to be investigated further. Only MPA, LPA, and RPA are included in this study and any effects due to higher order branching systems are not considered. Interpatient variability is an important issue and requires significant effort in obtaining precise data in infants and small children. We have put such efforts into place and are collecting data but this is a slow process that will take several months to obtain a reasonable number of patient data points.

Residual stress was not included in this work. Effect of residual stress in blood vessels has been studied extensively in the literature both experimentally and theoretically [30,31,19,32,29,20], mainly for the purpose of understanding remodeling in the blood vessel walls and the ability of the vessel to adapt to mechanical loading. A common approach of including residual stress in cylindrical models is to form the cylinder (load-free condition) by closing an open sector (stress-free condition) [31,19,20,29]. The open angle of the sector is usually determined experimentally by cutting an unloaded ring segment radially and measuring the angle subtended between two lines originating from the midpoint of the inner wall to the tips of the inner wall [30]. Such studies have consistently shown that accounting for residual stress in the stress analysis of arteries under physiologic pressure substantially reduces the stress gradient in the circumferential and axial stress across the arterial wall. Using a similar approach, Delfino et al. [19] included residual stress in a 3D finite-element model of carotid artery bifurcation based on cutting cadaver specimens along different lines and observing their "opening" behavior. However this approach is difficult to realize when clinical data and/or complex 3D anatomy are involved.

In conclusion, this work represents the first application of a statistical mechanics based orthotropic hyperelastic model to the clinical study of PA mechanics. Finite-element modeling using material properties from our previous results of rats with PAH agrees reasonably with the clinical *P-D* response in children with PAH. Material orthotropy affects the stress/strain pattern and *P-D* response. Further studies including higher order branching, nonuniform pressure loading, addition of the adventitial layer as well as active elements simulating smooth muscle cell action and use of 3D images derived from MRI are underway.

Acknowledgment

This work was supported in part through grants from the NIH (HL 072738, HL 067393, MO1-RR00069), General Clinical Research Centers Program, and NCRR.

References

[1] Anthony, G., Durmowicz, M. D., and Stenmark, K. R., 1999, "Mechanisms of Structural Remodeling in Chronic Pulmonary Hypertension," Pediatr. Rev., **20**, pp. e91–e102.

[2] Lanning, C., Chen, S. Y., Hangsen, A., Chang, D., Chan, K. C., and Shandas, R., 2004, "Dynamic Three-dimensional Reconstruction and Modeling of Cardiovascular Anatomy in Children With Congenital Heart Disease Using Biplane Angiography," Biomed. Sci., **40**, pp. 200–205.

[3] DeGroff, C. G., Birnbaum, B., Shandas, R., Orlando, W., and Hertzberg, J. R., 2005, "Computational Simulations of the Total Cavo-Pulmonary Connection: Insights Into Optimizing Numerical Solutions," Pediatr. Cardiol., **27**, pp. 135–146.

[4] Rashid, A., and Ivy, D., 2005, "Severe Paediatric Pulmonary Hypertension:

New Management Strategies," Arch. Dis. Child, **90**, pp. 92–98.
[5] Reuben, S. R., 1971, "Compliance of the Human Pulmonary Arterial System in Disease," Circ. Res., **29**, pp. 40–50.
[6] Harned, H. S., Jr., 1990, "Physiology of the Heart," *Pediatric Pulmonary Heart Disease*, Lippincott Williams & Wilkins Little, pp. 55–77.
[7] Tozzi, C. A., Christiansen, D. L., Poiani, G. J., and Riley, D. J., 1994, "Excess Collagen in Hypertensive Pulmonary Arteries Decreases Vascular Distensibility," Am. J. Respir. Crit. Care Med., **149**, pp. 1317–1326.
[8] Gibbons, G. H., and Dzau, V. J., 1994, "The Emerging Concept of Vascular Remodeling," N. Engl. J. Med., **330**, pp. 1431–1438.
[9] Shandas, R., Weinberg, C., Ivy, D. D., Nicol, E., DeGroff, C. G., Hertzberg, J., and Valdes-Cruz, L., 2001, "Development of a Non-Invasive Ultrasound Color M-mode Means of Estimating Pulmonary Vascular Resistance in Pediatric Pulmonary Hypertension: Mathematical Analysis, In vitro Validation, and Preliminary Clinical Studies," Circulation, **104**, pp. 908–913.
[10] Weinberg, C., Hertzberg, J. R., Ivy, D. D., Kirby, K. S., Chan, K. C., Valdes-Cruz, L. M., and Shandas, R., 2004, "Extraction of Pulmonary Vascular Compliance, PVR and RV Work From Single-Pressure and Doppler Flow Measurements in Children With Pulmonary Hypertension—A New Method for Evaluating Reactivity: In vitro and Clinical Studies," Circulation, **110**, pp. 2609–2617.
[11] Das, B. B., Bright, J. M., Boon, J. A., Yao, H. M., Lanning, C. J., Valdes-Cruz, L. M., and Shandas, R., 2004, "Use of Color M-mode Tissue Doppler Imaging to Calculate Dynamic Compliance of the Pulmonary Arteries in Pulmonary Hypertension: Validation in an Animal Model," J. Am. Coll. Cardiol., **43**, pp. 320A-320A, supplements.
[12] Dyer, K. L., Lanning, C., Das, B., Lee, P. F., Ivy, D. D., Valdes-Cruz L. M., and Shandas, R., 2006, "Noninvasive Doppler Tissue Measurement of Pulmonary Artery Compliance in Children With Pulmonary Hypertension," J. Am. Soc. Echocardiogr, **19**, pp. 403–412.
[13] Zhang, Y., Dunn, M. L., Drexler, E. S., McCowan, C. N., Slifka, A. J., Ivy, D. D., and Shandas, R., 2005, "Implementation and Application of a Microstructural Orthotropic Hyperelastic Model of Pulmonary Artery Mechanics under Normotensive and Hypertensive Conditions," Ann. Biomed. Eng., **33**, pp. 1042–1052.
[14] Arruda, E. M. and Boyce, M. C., 1993, "A Three-dimensional Constitutive Model for the Larger Stretch Behavior of Rubber Elastic Materials," J. Mech. Phys. Solids, **41**, pp. 389–412.
[15] Bischoff, J. E., Arruda, E. A., and Grosh, K., 2002, "A Microstructurally Based Orthotropic Hyperelastic Constitutive Law," J. Appl. Mech., **69**, pp. 570–579.
[16] Hibbitt, Karlsson & Sorensen, Inc., 2003, *ABAQUS/Standard Users Manual*, Version 6.4.
[17] Chen, S. Y. J., and Carroll, J. D., 2000, "3-D Reconstruction of Coronary Arterial Tree to Optimize Angiographic Visualization," IEEE Trans. Med. Imaging, **19**, pp. 318–336.
[18] Rodes-Cabau, J., Domingo, E., Roman, A., Majo, J., Lara, B., Padilla, F., Anivarro, I., Angel, J., Taradif, J. C., and Soler-Soler, J., 2003, "Intravascular Ultrasound of the Elastic Pulmonary Arteries: A New Approach for the Evaluation of Primary Pulmonary Hypertension," Heart, **89**, pp. 311–316.
[19] Delfino, A., Stergiopulos, N., Moore, J. E., and Meister, J. J., 1997, "Residual Strain Effects on the Stress Field in a Thick Wall Finite Element Model of the Human Carotid Bifurcation," J. Biomech., **30**, pp. 777–786.
[20] Raghavan, M. L., Trivedi, S., Nagaraj, A., McPherson, D. D., and Chandran, K. B., 2004, "Three-dimensional Finite Element Analysis of Residual Stress in Arteries," Ann. Biomed. Eng., **32**, pp. 257–263.
[21] von Maltzahn, W. W., Warriyar, R. G., and Keitzer, W. F., 1984, "Experimental Measurements of Elastic Properties of Media and Adventitia of Bovine Carotid Arteries," J. Biomech., **17**, pp. 839–847.
[22] Yu, Q., Zhou, J., and Fung, Y. C., 1993, "Neutral Axis Location in Bending and Young's Modulus of Different Layers of Arterial Wall," Am. J. Physiol., **265**, pp. H52-H60.
[23] Xie, J., Zhou, J., and Fung, Y. C., 1995, "Bending of Blood Vessel Wall: Stress-Strain Laws of the Intima-Media and Adventitial Layers," J. Biomed. Eng., **117**, pp. 136–145.
[24] Stefanadis, C., Dernellis, J., Vlachopoulos, C., Tsioufis, C., Tsiamis, E., Toutouzas, K., Pitsavos, C., and Toutouzas, P., 1997, "Aortic Function in Arterial Hypertension Determined by Pressure-Diameter Relation," Circulation, **96**, pp. 1853–1858.
[25] Stefandis, C., Tsiamis, E., Vlachopoulos, C., Stratos, C., Toutouzas, K., Pitsavos, C., Marakas, S., Boudoulas, H., and Toutouzas, P., 1997, "Unfavorable Effect of Smoking on the Elastic Properties of the Human Aorta," Circulation, **95**, pp. 31–38.
[26] Santana, D. B., Barra, J. G., Grignola, J. C., Gines, F. F., and Armentano, R. L., 2005, "Pulmonary Artery Smooth Muscle Activation Attenuates Arterial Dysfunction During Acute Pulmonary Hypertension," J. Appl. Physiol., **98**, pp. 605–613.
[27] Zhou, J., and Fung, Y. C., 1997, "The Degree of Nonlinearity and Anisotropy of Blood Vessel Elasticity," Proc. Natl. Acad. Sci. U.S.A., **94**, pp. 14255–14260.
[28] Drexler, E. S., McCowan, C. N., Wright, J. E., Slifka, A. J., Ivy, D. D., and Shandas, R., 2004, "Comparison of Strength Properties of Normotensive and Hypertensive Rat Pulmonary Arteries," Biomed. Sci. Instrum., **40**, pp. 297–302.
[29] Holzapfel, G. A., Gasser, T. C., and Ogden, R. W., 2000, "A New Constitutive Framework for Arterial Wall Mechanics and a Comparative Study of Material Models," J. Elast., **61**, pp. 1–48.
[30] Fung, Y. C., and Liu, S. Q., 1991, "Change of Zero-Stress State of Rat Pulmonary Arteries in Hypoxic Hypertension," J. Appl. Physiol., **70**, pp. 2455–2470.
[31] Fung, Y. C., and Liu, S. Q., 1992, "Strain Distribution in Small Blood Vessels With Zero-Stress State Taken Into Consideration," Am. J. Physiol., **262**, pp. H544–H552.
[32] Huang, W., and Yen, R. T., 1998, "Zero-Stress States of Human Pulmonary Arteries and Veins," J. Appl. Physiol., **85**, pp. 867–873.